DOI 10.1007/s11106-016-9792-1
Powder Metallurgy and Metal Ceramics, Vol. 55, Nos. 3-4, July, 2016 (Russian Original Vol. 55, Nos. 3-4, March-April, 2016)

REFRACTORY AND CERAMIC MATERIALS

STRUCTURAL AND MECHANICAL PROPERTIES OF BIOACTIVE GLASS–CERAMIC COMPOSITES

O. R. Parkhomei,[1] N. D. Pinchuk,[1,2] O. E. Sych,[1] T. V. Tomila,[1] G. B. Tovstonog,[1] V. F. Gorban',[1] Ya. I. Yevych,[1] and O. A. Kuda[1]

UDC 66.017:546.185′41:666.1:617

Bioactive glass–ceramic composites based on biogenic hydroxyapatite or synthetic calcium phosphates mixture with addition of sodium borosilicate glass (31.5 wt.%) are prepared using one-stage sintering at a temperature of ≤800°C. The comparative analysis of the structure and physical and mechanical properties of the composites produced is carried out. It is established that hydroxyapatite keeps the phase composition ($Ca_5(PO_4)_3(OH)$) during sintering of the biogenic hydroxyapatite-based composites. During sintering of the composites based on a mixture of synthetic phosphates, a phase transformation and interaction of phosphates with a glass phase occur. This results in the formation of glass ceramics, which contain: calcium silicates (wollastonite $CaSiO_3$) and sodium silicates ($Na_6Si_2O_7$), sodium-calcium silicates (sodium metasilicate $Na_2Ca_2(SiO_3)_3$ and melilite $Na_2Ca_6(Si_2O_7)(SiO_4)_2$), sodium borate ($Na_3BO_3$), and hydroxyapatite ($Ca_5(PO_4)_3(OH)$. The analysis of porous structure of glass–ceramic composites showed a significant difference in the pore size distribution, depending on the material composition. The difference in the surface and fracture structure for both types of composites is established. It is shown that the mechanical properties of the composites based on biogenic hydroxyapatite are higher compared to those based on synthetic calcium phosphates at the similar total porosity value (32.5–34.5%). This may be due to the phase transformations and interaction of phosphates with glass during sintering and the formation of a complex silica structure. It is established that the strength of the composites produced is comparable to that of the native bone.

Keywords: *hydroxyapatite, calcium phosphates, bioactive glass, composites, sintering, structure, porosity, strength.*

INTRODUCTION

In osteoplasty, the modern orthopedics and traumatology widely use the bioresorbable materials, which, after a certain period of time after implantation, are completely replaced with a new bone tissue of the patient. Such bioresorbable implants can be obtained based on: both synthetic and biogenic hydroxyapatite (HA), tribasic calcium

[1]Frantsevich Institute for Problems of Materials Science, National Academy of Sciences of Ukraine, Kiev, Ukraine.

[2]To whom correspondence should be addressed; e-mail: npinchuk@ukr.net.

Translated from Poroshkovaya Metallurgiya, Vol. 55, Nos. 3–4 (508), pp. 62–77, 2015. Original article submitted September 9, 2015.

phosphate, calcium pyrophosphate, bioglass, glass-ceramics, and polymers and various polymer-based composites [1–4].

In collaboration with colleagues-doctors [5–10], we have proven the advanced application of the developed and researched materials made of biogenic hydroxyapatite (BHA) in a pure form and in combination with sodium borosili borosilicate glass (SBSG) for the osteoplasty after traumatic bone defects and benign and malignant tumor-like diseases of the bones.

At the same time, we have shown [11] that obtaining BHA-based and ~50 wt.% SBSG-based composites using one-stage sintering at >650°C is very complicated. At this temperature, the materials are frothing, which, in turn, leads to the appearance of cracks and deformation of the samples (noticeable even to the naked eye), and to the transformation of the open porosity into the closed one (undesirable for implants). A two-stage sintering can prevent the above processes during obtaining the composites with a 50 wt.% glass phase. Using a mixture of synthetic calcium phosphates (SCP) in the form of phosphate component for producing SBSG composites [12, 13], we can obtain the implant samples of specified size and shape with no additional machining (volume shrinkage during sintering is <3%), which are effective in terms of the combination of high mechanical strength (108–150 MPa) and dissolution rate (0.25–0.58 wt.%/cm^2 · 24 h).

Since establishing of the structure–properties interrelationship allows adjusting and controlling the properties of implants, the study of structural and mechanical characteristics is one of the most important tasks of the modern materials science, including biomedical sector.

The purpose of this study is (i) to obtain glass–ceramic bioactive composites based on BHA or SCP mixture reinforced with 31.5 wt.% SBSG and (ii) to investigate their structure and physical and mechanical properties.

MATERIALS AND EXPERIMENTAL PROCEDURE

BHA, SCPs mixture, and SBSG were used as starting materials to produce glass–ceramic bioactive composites. BHA was obtained from the cattle bones by the technology described in [14]. The SCP mixture was obtained by chemical vapor deposition from solutions of calcium nitrate $Ca(NO_3)_2 \cdot 4N_2O$ (grade KhCh, Khimlaborreaktiv, Ukraine) and ammonium dihydrogen phosphate $(NH_4)H_2PO_4$ (grade KhCh, Khimlaborreaktiv, Ukraine). The resulting SCP powder consisted of: HA ($Ca_{10}(PO_4)_6(OH)_2$), β-tribasic calcium phosphate (β-TCP, β-$Ca_3(PO_4)_2$), tetrabasic calcium phosphate (TTCP, $Ca_4(PO_4)_2O$), and calcium pyrophosphate (CPP, $Ca_2P_2O_7$).

The SBSG (composition, wt.%: 49.10 SiO_2; 28.14 Na_2O; 22.76 B_2O_3) was obtained by cooking the charge with glass-forming components (using dry mixing on the mill table) at the maximum temperature of 1100ºC, with holding for 1 h, and subsequent cooling in the open air. Then, the cooked glass was re-melted at 1100°C (holding for 0.25 h) and poured into the water to obtain the frit, which was ground into the powder with a particle size of <160 μm.

The SBSG powder was employed in dry mixing with BHA or SCP (particle size <160 μm) to create composite systems. The charge contained 31.5 wt.% glass. The resulting was used to prepare cylindrical samples (dia. 15 mm) by dry compaction (under 150 MPa), which were sintered in the open air at ≤800ºC.

The following was determined for the samples produced: linear shrinkage in diameter $\Delta d/d_0$ and in height $\Delta h/h_0$; volume shrinkage $\Delta V/V_0$ during sintering; loss of mass $\Delta m/m_0$ during sintering; apparent density ρ; and porosity θ. The structure was examined by scanning electron microscopy (SEM) using a REM-106I (JSC SELMI, Ukraine). The images of the structures were processed using a SIAMS-600 image analysis system (SIAMS Ltd., Russia). The phase composition was examined by X-ray diffraction analysis using an Ultima IV diffractometer (Rigaku, Japan). In addition, the materials were studied by infrared (IR) spectroscopy using a FSM 1202 Fourier spectrometer (Infraspektr Ltd., Russia) in the frequency range of 4000–400 cm^{-1}.

To evaluate the mechanical properties, such as reduced modulus of indentation test (E_r), hardness (H_{IT}), pure elastic strain (ε_{es}), pure elastic stress (σ_{es}), the automatic indentation of materials was applied [15]. The compressive strength (failure stress σ_f) was determined by uniaxial compression using a Ceram Test System tester (Special Design Bureau at Pisarenko Institute for Problems of Strength, NAS of Ukraine).

RESULTS AND DISCUSSION

Figure 1 shows the XRD results of the starting powders (SBSG, BHA, and SCP) and BHA- and SCP-based glass–ceramic composites. Obviously, the SBSG is amorphous. BHA is represented only by HA ($Ca_5(PO_4)_3(OH)$ phase (JCPDS Card No. 9-432). SCP mixtures consist of: HA ($Ca_{10}(PO_4)_6(OH)_2$, JCPDS Card No. 9-432), β-tribasic calcium phosphate (β-$Ca_3(PO_4)_2$, JCPDS Card No. 32-0176), tetrabasic calcium phosphate ($Ca_4(PO_4)_2O$, JCPDS Card No. 25-1137), and calcium pyrophosphate ($Ca_2P_2O_7$, JCPDS Card No. 15-0197). When a glass is added into BHA to produce glass–ceramic composites and the samples are sintered at ≤800ºC, the X-ray diffraction pattern demonstrates nothing, but the HA ($Ca_5(PO_4)_3(OH)$ phase (JCPDS No. 9-432), indicating the BHA thermal stability under these conditions. However, in the case of sintering the composites, whose starting mixture contains SCP and SBSG, phase transformations occur and calcium phosphates interact with the glass. As a result, a multiphase material is formed. This material contains: sodium-calcium silicates, i.e., melilite ($Na_2Ca_6(Si_2O_7)(SiO_4)_2$, JCPDS Card No. 80-1296) and sodium metasilicate ($Na_2Ca_2(SiO_3)_3$, JCPDS Card No. 02-0961); calcium silicates, i.e., wollastonite ($CaSiO_3$, JCPDS Card No. 27-1064); sodium silicate ($Na_6Si_2O_7$, JCPDS Card No. 27-0784); sodium borate (Na_3BO_3, JCPDS Card No. 32-1047); and HA ($Ca_5(PO_4)_3(OH)$, JCPDS Card No. 9-432). Such behavior (during the interaction of the glass with SCP) can be attributed to the fact that the starting synthetic phosphates, namely synthetic HA, β-TCP, TTCP, and CPP are prone to phase transformations. This contributes to the formation of more reactive material with chemically active centers that lead to the interaction of phosphate component with the glass and the formation of chain and band silicates in the material.

The XRD results are also confirmed by IR-spectrometry (Fig. 2, Table 1). The IR absorption spectrum of the BHA composite is a superposition of the BHA and SBSG spectra. It possesses a set of absorption bands typical for HA (vibrations of major structure components, such as: PO_4^{3-} (1092, 1041, 960, 603, 567, and 472 cm^{-1}) and OH^- (3568, 3440, and 1631 cm^{-1})) and SBSG (frequency of B—O asymmetric valence vibrations in the boron trigonal coordination (BO_3^-) is $\nu \approx 1500–1390$ cm^{-1}, B—O—B strain vibrations is $\nu \approx 701$ cm^{-1}, and vibrations of tetrahedrons BO_4^- is $\nu \approx 966$ cm^{-1} [16]).

An expansion of all absorption bands with regard to the BHA starting sample is observed in the IR absorption spectrum of the BHA composite. In the frequency range $\nu \approx 900–700$ cm^{-1}, new absorption bands appear starting from $\nu \approx 849$ cm^{-1} (this band referred to as B—O vibrations) and $\nu \approx 750$ and 710 cm^{-1} that characterize the P—O—P and B—O—B vibrations, respectively. In addition, a change in the fine structure of the bands in the range of $\nu \approx 1550–1300$ cm^{-1} and the broad bands of average intensity with frequencies $\nu \approx 1460$ cm^{-1} and $\nu \approx$ ≈ 1396 cm^{-1}, which are biased against the absorption bands of the starting glass and BHA, are observed in the IR absorption spectrum of the composite. Also, low-intensity bands in the range of $\nu \approx 770–650$ cm^{-1} characterize the vibrations of X_2O_7 type structures (where X = Si, P) [17]. Neither pyrophosphates nor pyrosilicates were XRD-identified and, therefore, we can assume an insignificant presence of such textural features. The disappearance of the absorption band of liberations OH^- at $\nu \approx 632$ cm^{-1} (Table 1) in relation to the spectrum of the starting specimens indicates the formation of the BHA composite and SBSG.

The analysis of the IR spectrum of the SBSG and SCP composite indicates the formation of multiphase composite (Fig. 2; Table 1), which is also XRD-confirmed. The overlapping of characteristic absorption band areas is inherent to the IR spectrum of the composite. Therefore, to identify the phase composition, we have identified only the bands that do not overlap, *hereinafter referred to as* "the reference bands" for each type of structural groups. The formation of sodium–calcium silicate $Na_2Ca_6(Si_2O_7) \cdot (SiO_4)_2$ characterizes the absorption reference bands with frequencies $\nu \approx 1005$, 825, 525 cm^{-1} and $\nu \approx 915$, 756 cm^{-1}, indicating the presence of vibrations of the groups SiO_4 and Si_2O_7, respectively [17]. The absorption bands at $\nu \approx 1035$ and 945 cm^{-1} characterize the presence of metasilicate chains $(SiO_3)_n$, belonging to wollastonite structures. The absorption bands at $\nu \approx 1400–1200$ cm^{-1} can be ascribed to the B—O valence symmetric and asymmetric vibrations, while the absorption bands at $\nu \approx$ ≈ 706 cm^{-1} can be ascribed to the B—O—B strain vibrations in the boron trigonal coordination (BO_3^-) indicating the formation of sodium borate $NaBO_3$. The weak absorption band $\nu \approx 773$ cm^{-1} characterizes the vibrations of the

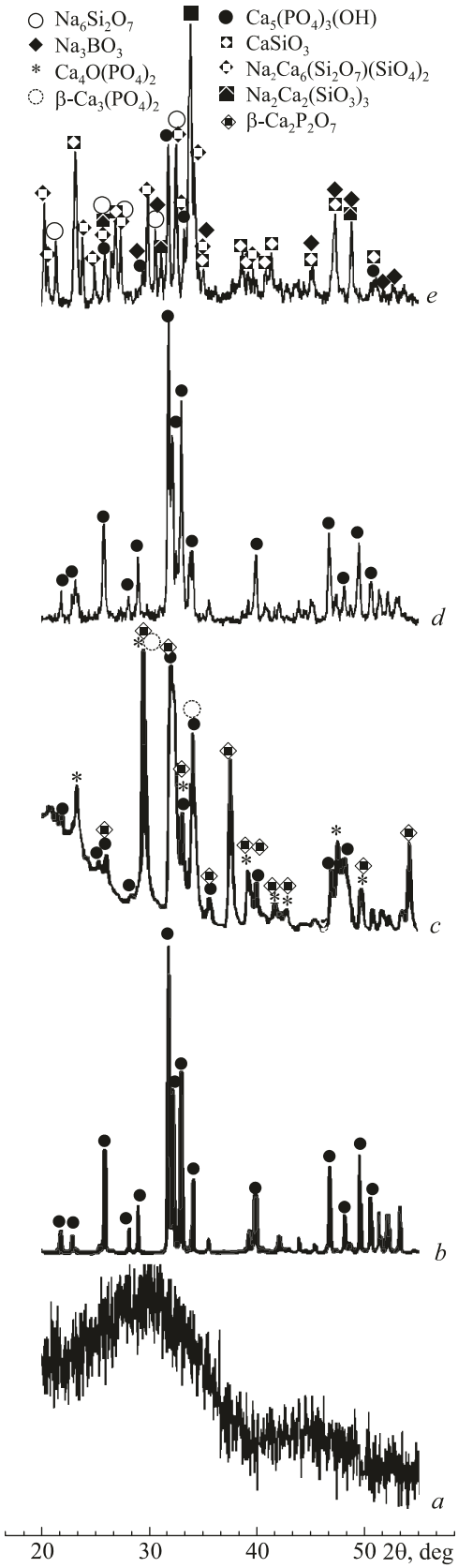

Fig. 1. XRD results for SBSG (*a*), BHA (*b*), and SCP (*c*), as well as for BHA (*d*) and SCP (*d*) based glass–ceramic composites

TABLE 1. Frequencies of the IR Absorption Bands of the SBSG, BHA, and SCP Specimens, and also of the BHA- and SCP-Based Glass–Ceramic Composites

Material	ν_1	ν_2	ν_3	ν_4	ν_5	ν_6	ν_7	ν_8	ν_9
SBSG	470m.w.	–	–	–	–	701m.w.	–	–	850w.
BHA	472w.	–	570s.n.	604s.n.	632m.n.	–	–	800w.	871w.n.
SCP	470w.	–	566s.n.	602s.n.	631m.n.	702s.wk.	726s.wk.	848m.n.	873m.n.
BHA composite	472w.	–	567s.n.	603m.n.	–	710w.	750w.	775s.wk.	849med.
SCP composite	461med.	525w.n.	573m.n.	604med.	–	706med.	756w.	773w.	825m.n.
Material	ν_{10}	ν_{11}	ν_{12}	ν_{13}	ν_{14}	ν_{15}	ν_{16}	ν_{17}	ν_{18}
SBSG	966s.wd.	–	1060s.wd.	–	–	–	–	–	–
BHA	961m.n.	–	1051s.n.	1090s.n.	–	–	1262w.	–	1385s.wk.
SCP	963med.	–	1052s.	1091s.	–	–	–	1270m.n.	1384s.
BHA composite	960med.	–	1041s.	1092s.	–	–	–	–	–
SCP composite	945m.n. 915sh.	1005s.	1035s.	1080s.	1130med.	1220s.wk.	1253w.	1281med.	1350med.
Material	ν_{19}	ν_{20}	ν_{21}	ν_{22}	ν_{23}	ν_{24}	ν_{25}	ν_{26}	ν_{27}
SBSG	1408m.w.	–	1471m.w.	1635med.	2854s.wk.	2925s.wk.	–	3442s.wd.	–
BHA	1416 w.n.	1458m.n.	1549w.n.	1632m.w.	–	–	–	3440m.w.	3568w.n.
SCP	1406 s.	1433s.	1557med.	1635med. 1660med.	2783w. 2851med.	2922med.	3364 m.w.	–	3571w.n. 3643m.n.
BHA composite	1396m.w.	1460m.w.	–	1631w.w.	–	–	–	3440m.w.	3568s.wk.
SCP composite	1386s.wk.	1427med.	1475med.	1638med. 1657med.	–	3030w.w.	3360s.wd.	3440s.wd.	–

Remarks: s. means strong; s.n. means strong narrow; s.wd. means strong wide; med. means medium; m.n. means medium narrow; m.w. means medium wide; w. means weak; s.wk. means strong weak; w.n. means weak narrow; w.w. means weak wide; sh. means shoulder.

P_2O_7 anion in pyrophosphate structures and indicates the presence of β-$Ca_2P_2O_7$ [18], while the absorption frequency $\nu \approx 1130$ cm^{-1} is a reference band to identify the phase of tribasic calcium phosphate β-$Ca_3(PO_4)_2$. The presence of the last two phases in the composite structure can be associated with remains of the starting phosphates, which have not reacted during the formation of the composite structure.

The IR spectra of the starting phosphates and both types of the composites possess the absorption bands typical for the vibrations of the carbonate group CO_3^{2-} in the frequency range $\nu \approx 1475$–1400 cm^{-1} and $\nu \approx 850$ cm^{-1}. It should be noted that the carbonate ions in the BHA and SCP structure (Fig. 2) are in both A-position (replacement groups OH^-) and B-position (replacement groups PO_4^{3-}). In the case of composites, it remains only a small amount of carbonates adsorbed from the air. The XRD has found no carbonates. Therefore, we can assume that the number of such structures is negligible and they belong to the remains of the starting components.

During sintering, glass–ceramic specimens undergo not only phase transformations, but also linear changes, volume changes, and loss of weight. Table 2 shows that the volume shrinkage of the SCP glass–ceramic composites exceeds that of the BHA glass–ceramic composites, by a factor of 3. It has to do with phase transformations and recrystallization in the material, though the loss of weight for both composites is very close. Table 2 displays the density and porosity of the materials. The density of the BHA composites is higher than that of the SCP composites, which can also be explained by phase interactions and transformations during the sintering of the SCP composites. In comparison with the BHA composites, the total porosity of the SCP composites is slightly higher. This is caused by phase transformations during the sintering and redistribution of the pore space (or vacancy phase). At the same time, the open porosity of the composites is significantly different. The open porosity prevails in the SCP-based

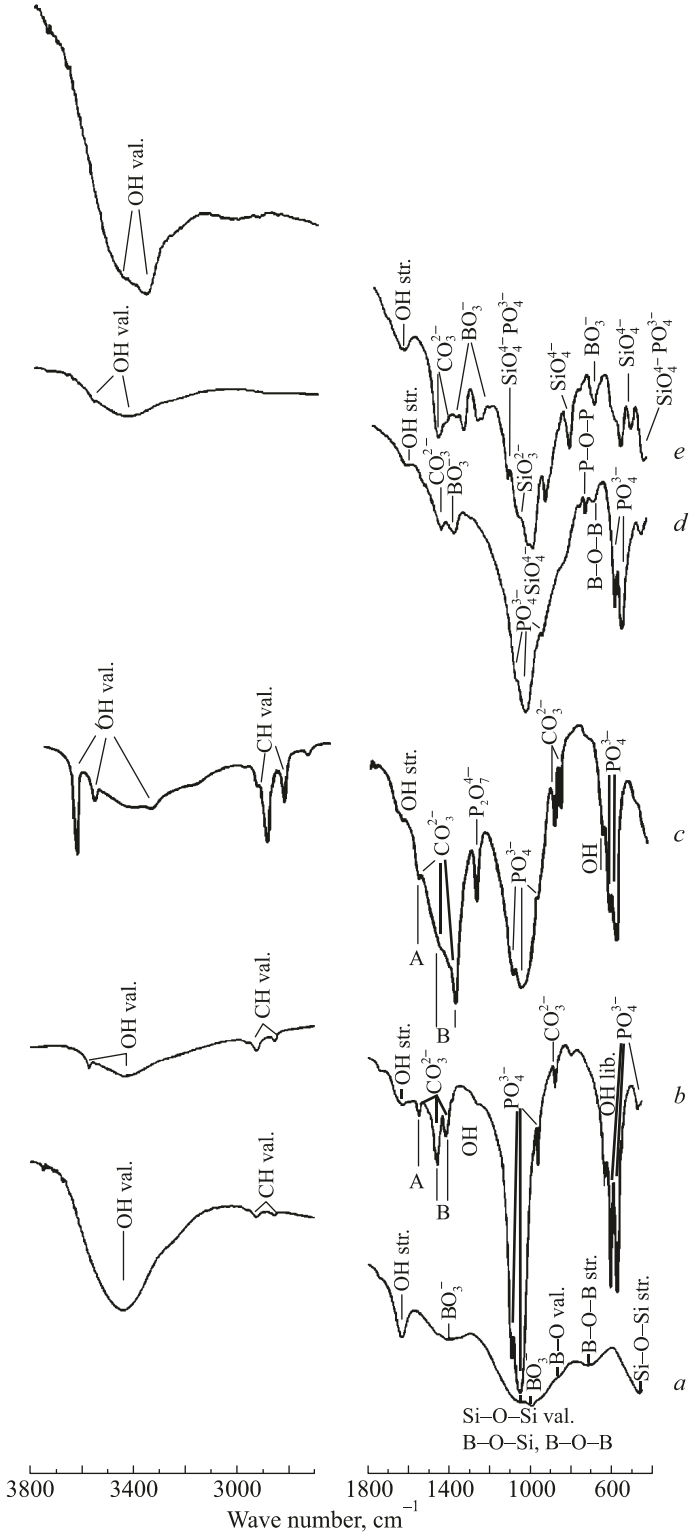

Fig. 2. IR-spectra of SBSG (*a*), BHA (*b*), and SCP (*c*), as well as of BHA (*d*) and SCP (*e*) based glass–ceramic composites (val., str., and lib. stand for valence, strain, and liberations, respectively)

specimens, while it reaches only 4.4% in the BHA-based specimens. This may be due to the glass properties and the peculiarities of the sintering of composites, resulting in the formation of a glassed surface and a structure with isolated pores.

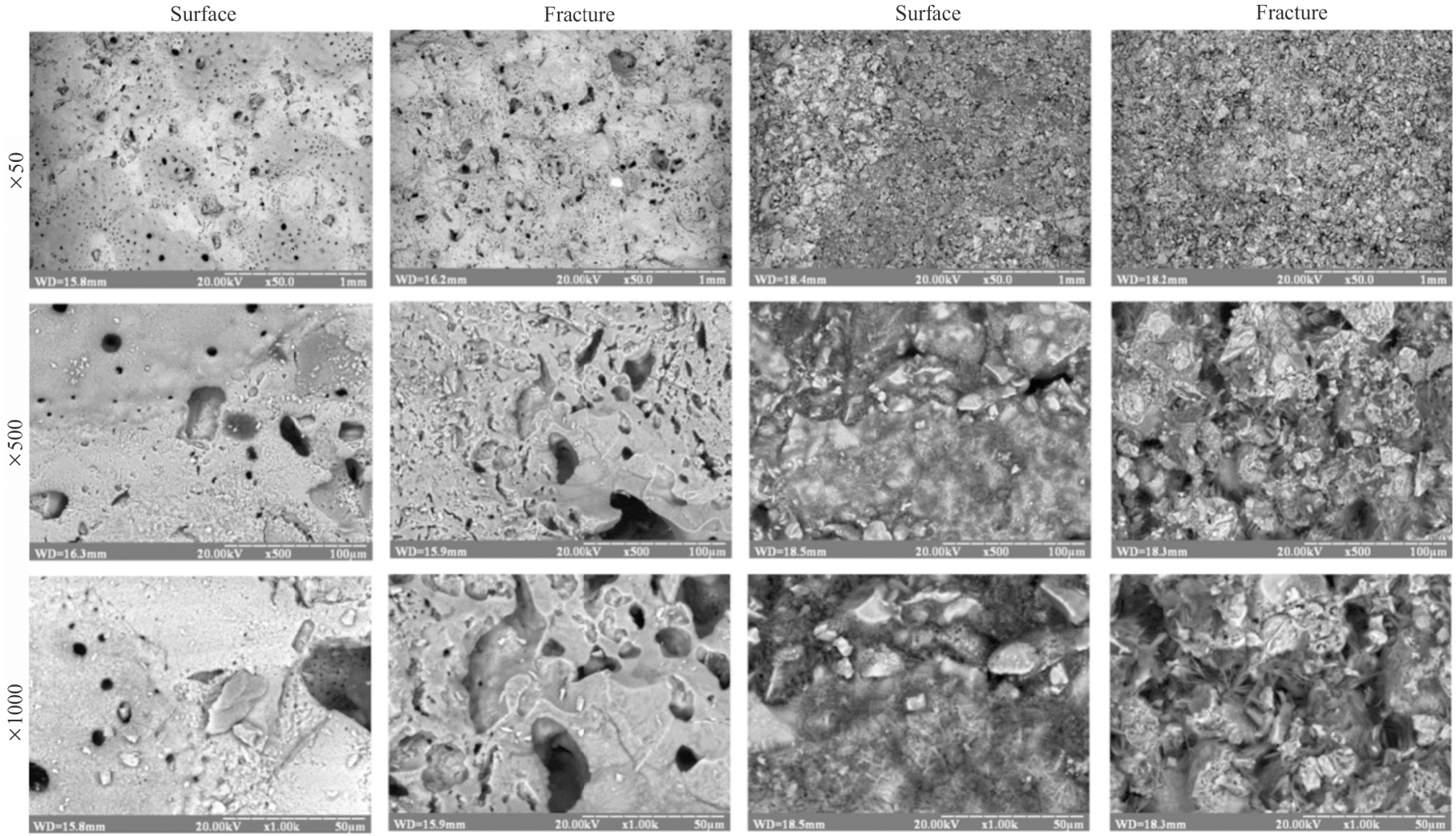

Fig. 3. BHA (*a*) and SCP (*b*) based glass–ceramic composites: structure of the surface and fracture of the specimens

TABLE 2. Parameters of the BHA and SCP Based Glass–Ceramic Composites after Sintering

Type of phosphate	$\Delta h/h_0$, %	$\Delta d/d_0$, %	$\Delta V/V_0$, %	$\Delta m/m_0$, %	ρ, g/cm^3	θ, %	
						Total	Open
BHA	0.41	0.51	1.62	0.35	1.91	32.5	4.4
SCP	2.13	0.98	4.25	0.55	1.76	34.5	24.1

Figure 3 shows that the structure of the surface and fracture of the BHA- and SCP-based glass–ceramic composites is significantly different. Both types of composites possess a porous surface structure, but only the surface of the BHA-based samples is glassed, due to the properties of the SBSG. At the sintering temperature, when the glass mass is in the viscous-fluid state, it occurs almost complete wetting of BHA with the glass mass that, together with the forces of surface tension, forms a glassed surface of the samples. In addition, small and rather large pores are seen both on the surface and at the fracture of the specimens of BHA-based glass–ceramic composites. Such a heterogeneous structure can also result from the "impact" of the glass mass on the sintering. It is known that the glass mass absorbs a large amount of gases from air during cooking; these gases may be removed during the second heating. At the sintering temperature, the viscosity of the glass mass (Fig. 4) is still too high to completely remove all gaseous products from the material, because the total outgassing may occur when the logarithmic viscosity number equals to 2 [19]. Note that the heterogeneous porous structure is formed not only on the surface, but also across the sample. In the case of SCP-based glass–ceramic composites, such a glassed surface is not observed. This may be associated with phase transformations, the interaction of the glass mass with phosphates during sintering, and recrystallization of the material.

In addition, it is established that the type of the starting phosphate component greatly affects the shape of grains in the material. Phase transformations result in the formation of typical-for-wollastonite "grains–needles" in the structure of SCP composites after the thermal treatment of the material. Figure 5 shows the grain-size distribution

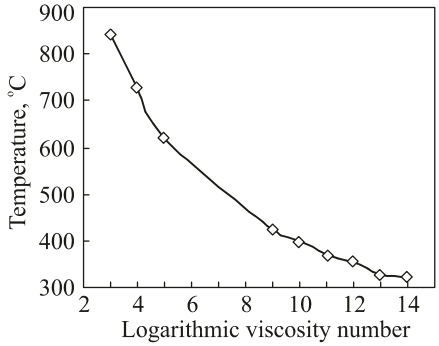

Fig. 4. Temperature–viscosity diagram for SBSG

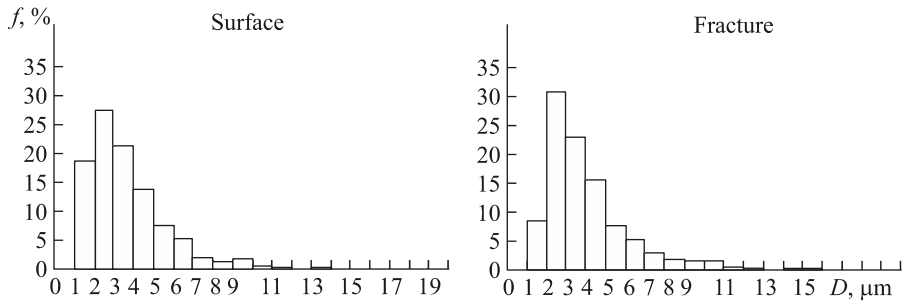

Fig. 5. SCP-based glass–ceramic composites: grain-size distribution in the structure of the surface and fracture

TABLE 3. Test Results of the Grain and Pore Structure of BHA- and SCP-Based Glass–Ceramic Composites

Material	Size, μm			Mean square deviation, μm	Coefficient of variation
	Minimum	Maximum	Median		
Grain structure					
SCP:					
surface	1.01	19.55	3.66	2.09	0.57
fracture	1.26	17.13	4.08	2.29	0.56
Pore structure					
BHA:					
surface	1.47	113.14	9.23	11.44	1.24
fracture	0.96	152.21	4.67	8.36	1.79
SCP:					
surface	0.60	26.70	3.95	4.35	1.10
fracture	2.07	67.32	8.83	7.98	0.90

and Table 3 shows the results of the grain structure analysis of the surface and fracture of the specimens containing SCP in their starting composition. In general, the grains are 1.0–19.5 μm in size. If the mean square deviation and the parameter of the grain structure homogeneity (coefficient of variation) have close values, the minimum and median size of grains are smaller on the surface, while the maximum size of grains is smaller in the fracture of the composite specimens. Most of the grains of the composite surface are 1–5 μm in size, whereas 80% of grains in the fracture are 2–5 μm in size. In addition, the structure contains heterogeneous agglomerates of various sizes, covered with a glass phase. It is difficult to distinguish individual grains in the BHA-based samples for the material being glassed.

Figure 6 and Table 3 show the results of the analysis of the porous structure, conducted using a SIAMS-600 image analysis system. The comparison of the porous structure of the BHA- and SCP-based glass–ceramic composites has revealed a significant difference not only in the pore-size distribution depending on the composition of the material, but also in the structures of the surface and fracture. In comparison with the BHA-based specimens, the size of the pores (minimum, maximum, and median) on the surface of the SCP-based specimens is smaller, by a factor of 2–2.3. In addition, the pore structure is more homogeneous, which is evidenced by the coefficient of

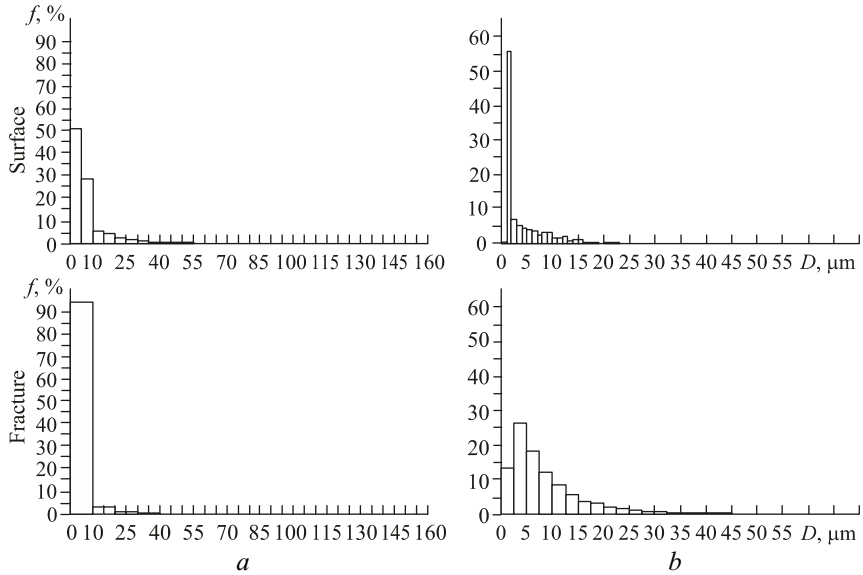

Fig. 6. BHA (*a*) and SCP (*b*) based glass–ceramic composites: grain-size distribution in the structure of the surface and fracture

variation (1.10 < 1.24). Most of the pores in BHA-based composites (80%) and SCP-based composites (58%) are 1.5–10.0 μm and 1–2 μm in size, respectively. Therefore, the pore distribution range is narrower on the surface of the SCP-based specimens.

Provided close values of mean square deviation, the minimum and median size of pores in the SCP-based composite fracture doubles that in the BHA-based composite fracture, while the maximum size of pores is smaller, by a factor of 2.3. The pore structure of the SCP-based specimens is more homogeneous, which is evidenced by the coefficient of variation (0.9 < 1.79). The pores (95%) in the BHA-based composites and the pores (68%) in the SCP-based composites are 1–10 μm and 2–10 μm in size, respectively. Therefore, the pore distribution range is narrower in the fracture of the BHA-based specimens.

The comparison of the structure of the surface and fracture of the SCP-based specimens reveals that the pore size on the surface (minimum, maximum, and median) is smaller than that in the fracture, by a factor of 2–3. However, a narrower pore-size distribution range on the surface of the material is seen: most of the surface pores (58%) and fracture pores (68%) are 1–2 μm and 2–10 μm in size, respectively.

Due to the glassed surface of the BHA-based composites, the minimum and median size of the fracture pores are smaller than those of the surface pores and, on the contrary, the maximum size is smaller with the surface pores. This may be caused by degassing processes during liquid phase sintering. Most of the surface pores (80%) and fracture pores (95%) of the samples are 1.5–10.0 μm and 1–10 μm in size, respectively, i.e., the fracture possesses a narrower pore-size distribution range.

In general, the surface and fracture pores in the SCP-based composites are 0.6–26.7 μm and 2.1–67.3 μm in size, respectively, and those in the BHA-based composites are 1.5–113.1 μm and 1.0–152.2 μm in size, respectively.

An approach for processing and analyzing the results of the instrumented indentation of materials according to ISO 14577-1:2002 (E) is discussed in [20, 21]. The approach is based on an analytically obtained equation for indentation that sets a functional relationship between the strength and strain properties and the indexes of automatically recorded diagram. Given that the flow stress of material depends on the structural condition (the Hall–Petch equation), the relationship between the H_{IT}/E_r pattern and the structural condition of materials has been established.

TABLE 4. Structural and Mechanical Characteristics of BHA- and SCP-Based Glass–Ceramic Composites

Type of phosphate	σ_f, MPa	H_{IT}, GPa	E_r, GPa	ε_{es}, %	σ_{es}, MPa	H_{IT}/E_r
BHA	67	0.63	23	0.84	193	0.027
SCP	54	0.43	17	–	130	0.025

Table 4 lists the mechanical chracteristics obtained from the calculations based on the automatic indentation diagrams of the composite specimens. All the mechanical characteristics of the BGA-based composites are higher, than those of the SCP-based composites. Herewith, both materials possess a fine-crystalline structure, which was determined using the ratio H_{IT}/E_r. The difference in parameters σ_f and σ_{es} can be explained by the fact that the degree of σ_{es} was determined at the strain of 9.8% (data received at the angle of sharpening of the Berkovich pyramid).

According to the XRD and IR spectroscopy, the presence of chemically active glass phase during synthesis of composites leads to its interaction with the crystalline phases of calcium phosphates. During the sintering of composites, an active formation of silicates occurs accompanied with a release of new crystalline phases, which is particularly noticeable in the SCP-based composite. During its synthesis, the formation and crystallization of the chain and band silicates with complex structure in some way affects the structural and mechanical properties, unlike the BGA-based composites where HA is a more stable crystalline phase. The formation of the nucleus and heterogeneous structure of several crystalline phases in the presence of significant size cations Ca^{2+} and Na^{+} (based

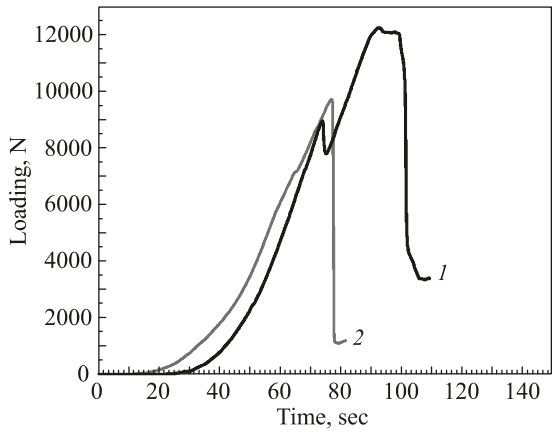

Fig. 7. Loading diagram during compression of BHA (*1*) and SCP (*2*) based glass–ceramic composites

on wollastonite chains of tetrahedrons [SiO_4] and band silicates of [Si_2O_7] groups) causes the degradation in the structural and mechanical properties. This is typical for the SCP-based composites, unlike the BHA-based composites, at close values of total porosity (Table 4).

Figure 7 shows the results of specimens testing during uniaxial compression that confirm the data obtained by indentation method. The loading diagrams demonstrate that the failure of both type of the specimens is brittle, however, the BHA-based specimens do not only have a greater strength of σ_f (Table 2), but longer resist the failure. Herewith, the total porosity of the materials is close on values, but unlike the SCP-based composites, the porosity of the BHA-based composites is mostly closed. Therefore, the BHA-based composites have a higher performance of compressive strength, because, given the same total porosity, the structure with isolated pores is more durable due to the higher degree of the matrix structure. In general, the strength of the glass–ceramic composites produced is close to that of the natural (native) bones [22].

CONCLUSIONS

Glass–ceramic composite materials based on the calcium-phosphate component (biogenic hydroxyapatite or mixture of synthetic calcium phosphates), strengthened with the sodium borosilicate glass (31.5 wt.%) have been produced by one-stage sintering at a temperature of ≤800°C. Depending on the type of the calcium-phosphate component, certain differences have been established based on the research of the structure and physical and mechanical properties of the composites.

It has been established that the crystalline phase of hydroxyapatite ($Ca_5(PO_4)_3(OH)$) is preserved during sintering the BHA-based composites. During sintering, the composite materials with a SCP mixture in the starting composition undergo phase transformations and phosphates interact with the glass phase. These processes result in the formation of glass–ceramic composites, which contains sodium-calcium silicates, i.e., melilite ($Na_2Ca_6(Si_2O_7)(SiO_4)_2$) and sodium metasilicate ($Na_2Ca_2(SiO_3)_3$); calcium silicates (wollastonite $CaSiO_3$); sodium silicate ($Na_6Si_2O_7$); sodium borate (Na_3BO); and hydroxyapatite ($Ca_5(PO_4)_3(OH)$). The data have been confirmed by IR-spectrometry.

Based on the analysis of the microstructure of the composites, it has been established that the type of the starting phosphate component greatly affects the sintering and the grain shape of the material. The phase transformations result in the formation of grains–needles (1.0–19.5 μm) in the SCP-based composites. Such grains are typical for wollastonite, and individual grains can be hardly distinguished in the BHA-based composites for the material being glassed.

In addition, the study of the porous structure of glass–ceramic composites has revealed a significant difference in the pore-size distribution, depending on the composition of the samples. Also, the difference in the structure of the surface and fracture for both types of the composites has been determined. The porosity of the fracture of both composites is higher than that of the surface by one order of magnitude, because it is glassed, as a

result of the sintering. The pore structure of the surface and fracture of the SCP samples is more homogeneous in comparison with those based on biogenic hydroxyapatite. In general, the surface and fracture pores in the SCP-based composites are 0.6–26.7 μm and 2.1–67.3 μm in size, respectively, and those in the BHA-based composites are 1.5–113.1 μm and 1.0–152.2 μm in size, respectively. The total porosity of the BHA-based and SCP-based samples is 32.5% and 34.5%, respectively.

It has been established that, at close values of the total porosity, the mechanical properties of the BHA-based composites are higher, than those of the SCP-based composites. It can be explained by phase transformations, the interaction of phosphates with the glass during the sintering of the SCP-based composites, and the formation of the complex silicate structure. Note that the compression strength (54–65 MPa) of the glass–ceramic composites produced is close to the strength of the natural (native) bone.

ACKNOWLEDGEMENTS

The authors are grateful to L. A. Ivanchenko for consulting, when planning experiments.

REFERENCES

1. T. V. Safronova and V. I. Putlyaev, "Medical inorganic materials science in Russia: calcium phosphate materials," *Nanosistemy: Fiz. Khim. Matemat.*, **4**, No. 1, 24–47 (2013).
2. M. Sadat-Shojai, M. T. Khorasani, E. Dinpanah-Khoshdargi, and A. Jamshidi, "Synthesis methods for nanosized hydroxyapatite with diverse structures," *Acta Biomater.*, **9**, No. 8, 7591–7621 (2013).
3. E. C. Hammel, O. L.-R. Ighodaro, and O. I. Okoli, "Processing and properties of advanced porous ceramics: an application based review," *Ceram. Int.*, **40**, No. 10, 15351–15370 (2014).
4. M. Šupová, "Substituted hydroxyapatites for biomedical applications: a review," *Ceram. Int.*, **41**, No. 8, 9203–9231 (2015).
5. E. P. Podrushnyak, L. A. Ivanchenko, T. I. Fal'kovs'ka, et al., "New bio-composites based on the bone hydroxyapatite and their applicability in biology and medicine," *Probl. Osteol.*, **1**, Nos. 2–3, 98–100 (1998).
6. V. I. Luzin, S. V. Petrosyants, Yu. S. Plyaskova, et al., "The chemical composition of the various divisions of long tubular bones during grafting of the biogenic hydroxyapatite," *Travma*, **10**, No. 3, 346–350 (2009).
7. D. V. Ivchenko, "Tactics of treatment of pathologic fractures of the extremities in patients with benign and malignant-like tumors," *Ortoped. Travmatol. Protezir.*, No. 4, 12–15 (2006).
8. V. I. Luzin and A. A. Lubinets, "The growth, structure, and shaping bones when grafting biogenic hydroxyapatite doped with manganese different contents into the tibia," *Ukr. Morfolog. Al'manakh*, **9**, No. 3, 116–117 (2011).
9. N. D. Pinchuk, A. R. Parkhomei, A. A. Kuda, and L. A. Ivanchenko, "Composite coatings from bioactive calcium phosphate ceramics on metals substrates," *Powder Metall. Met. Ceram.*, **53**, Nos. 1–2, 40–47 (2014).
10. G. B. Tovstonog, O. E. Sych, and V. V. Skorokhod, "Structure and properties of biogenic hydroxyapatite ceramics: microwave and conventional sintering," *Powder Metall. Met. Ceram.*, **53**, Nos. 9–10, 566–573 (2014).
11. E. E. Sych, N. D. Pinchuk, and L. A. Ivanchenko, "Effect of sintering temperature on the properties of biogenic hydroxyapatite–glass composites," *Powder Metall. Met. Ceram.*, **49**, Nos. 3–4, 153–158 (2010).
12. O. E. Sych, N. D. Pinchuk, L. A. Ivanchenko, and O. R. Parkhomei, *Calcium–Phosphate Composite Biomaterial*, Ukrainian Patent on Useful Model 43042 Ukraine, MPK A61K 33/42, A61P 19/00. Applicant and Owner: Frantsevich Institute for Problems of Materials Science, NAS of Ukraine, No. u200902943; Appl. 30.03.2009; Publ. 27.07.2009, Bull. No. 14, p. 3.
13. O. E. Sych, *The Evolution of the Structure and Properties of Composite Materials Based on Calcium Phosphates Produced by Liquid-Phase Sintering* [in Ukrainian], PhD Thesis, Kyiv (2010), p. 20.

14. E. P. Podrushnyak, L. A. Ivanchenko, V. L. Ivanchenko, and N. D. Pinchuk, *Hydroxyapatite and its Production (Options)*, Ukrainian Patent 61938 Ukraine, MPK A61K35/32, A61K33/00, A61K6/02, A61P19/00. Applicant and Owner: E. P. Podrushnyak, L. A. Ivanchenko, V. L. Ivanchenko, No. 99095233; Appl. 21.09.1999; Publ. 15.12.2003, Bull. No. 12, p. 7.
15. S. A. Firstov, V. F. Gorban', and E. P. Pechkovskii, "New methodological approaches for determining the mechanical properties of modern materials by automatic indentation," *Nauka Innovats.*, **6**, No. 5, 7–18 (2010).
16. C. Gautam, A. K. Yadav, and A. K. Singh, "A review on infrared spectroscopy of borate glasses with effects of different additives," *Int. Scholarly Res. Network*, *Ceramics,* 1–17 (2012).
17. A. P. Lazarev, *Vibration Spectra and Silicate Structure* [in Russian], Nauka, Leningrad (1968), p. 346.
18. L. Berzina-Cimdina and N. Borodajenko, "Research of calcium phosphates using Fourier transform infrared spectroscopy," *Infrared Spectr. Mater. Sci. Eng. Technol.*, **6**, 123–148 (2012).
19. I. I. Kitaigorodskii, *Glass Production: Handbook in 3 Vols*. [in Russian], Gos. Izd. Lit. Stroit. Arkhitect. Stroit. Mater., Moscow (1963), Vol. 1, p. 1026.
20. S. A. Firstov, V. F. Gorban', E. P. Pechkovskii, and N. A. Memeka, "The relationship between strength characteristics and automatic indentation data," *Materialoved*., No. 11, 26–31 (2007).
21. V. F. Gorban' and E. P. Pechkovskii, "Instrumented indentation for determining the structural state of materials," *Powder Metall. Met. Ceram.*, **49**, Nos. 7–8, 424–429 (2010).
22. S. A. Goldstein, "The mechanical properties of trabecular bone: dependence on anatomic location and function," *J. Biomechan.*, **20**, Nos. 11–12, 1055–1061 (1987).